Received: 21 January 2017 | Accepted: 21 August 2017
DOI: 10.1002/jcp.26162

ORIGINAL RESEARCH ARTICLE

WILEY Journal of Cellular Physiology

Claudin7b is required for the formation and function of inner ear in zebrafish

Xiaohui Li[1,2] | Guili Song[1] | Yasong Zhao[1,2] | Feng Zhao[3] | Chunyan Liu[1] | Dong Liu[3] | Qing Li[1] | Zongbin Cui[1]

[1] State Key Laboratory of Freshwater Ecology and Biotechnology, Institute of Hydrobiology, Chinese Academy of Sciences, Wuhan, China

[2] University of Chinese Academy of Sciences, Beijing, China

[3] Department of Biology, Southern University of Science and Technology, Shenzhen, China

Correspondence
Zongbin Cui and Qing Li, State Key Laboratory of Freshwater Ecology and Biotechnology, Institute of Hydrobiology, Chinese Academy of Sciences, Wuhan 430072, China.
Email: zbcui@ihb.ac.cn (ZC); qli@ihb.ac.cn (QL)

Funding information
The National Natural Science Foundation of China, Grant number: 31571504; The National Basic Research Program of China, Grant number: 2012CB944500; The National Natural Science Foundation of China, Grant number: 31571496

Zebrafish has become an excellent model for studying the development and function of inner ear. We report here a zebrafish line in which *claudin 7b* (*cldn7b*) locus is interrupted by a Tol2 transposon at its first intron. The homozygous mutants have enlarged otocysts, smaller or no otoliths, slowly formed semicircular canals, and insensitiveness to sound stimulation. These abnormal phenotypes and hearing loss of inner ear could be mostly rescued by injection of *cldn7b*-mRNA into one-cell stage homozygous mutant embryos. Mechanistically, *cldn7b*-deficiency interrupted the formation of apical junction complexes (AJCs) in otic epithelial cells of inner ear and the ion-homeostasis of endolymph, which then led to the loss of proper contact between otoliths and normally developed hair cells in utricle and saccule or aberrant mechanosensory transduction. Thus, Cldn7b is essential for the formation and proper function of inner ear through its unique role in keeping an initial integrity of otic epithelia during zebrafish embryogenesis.

KEYWORDS
claudin7b, hearing loss, inner ear, tight junction, zebrafish

1 | INTRODUCTION

Mammalian ear is composed of external, middle, and inner ear portions. The inner ear is a conserved sensory organ that mediates both vestibular and auditory functions of vertebrate (Fritzsch & Beisel, 2001; Fritzsch, Pauley, & Beisel, 2006) and is important for detecting acceleration and keeping balance (Jarvis, Johnston, & Sulik, 1990). Teleost fish, such as the zebrafish, only possess the inner ear. Despite the considerable structure diversities of otocysts in different species, the molecular basis of their development is relatively conserved (Whitfield, Mburu, Hardisty-Hughes, & Brown, 2005). As a model vertebrate animal, zebrafish has been popularly used to investigate gene functions during inner ear development, largely due to its well established genetic tools (Han et al., 2011).

Morphologically, zebrafish inner ear starts as a two-cell width ectodermal thickness, called the otic placode, lateral to the developing hindbrain, at approximately 14.5 hours post-fertilization (hpf) (Kimmel, Ballard, Kimmel, Ullmann, & Schilling, 1995). After the cavitation of otic placode to form the otic vesicle at 18hpf, the first few mechanosensory hair cells appear at anterior and posterior sensory epithelium. Kinocilia of these newborn hair cells serve as the seed points for the calcium carbonate and otolith protein deposits. Both anterior and posterior otoliths become visible by 22hpf. Each otolith is inertial, in touch with hair cell kinocilia, and displacement of them deflects hair cell bundles to initiate auditory or vestibular circuitry (Inoue, Tanimoto, & Oda, 2013; Lundberg, Xu, Thiessen, & Kramer, 2015).

The first few hair cells are also called tether cells, known to be essential for otolith nuclei formation and positioning within the ear placode (Riley, Zhu, Janetopoulos, & Aufderheide, 1997). The swing of tether cell cilia is involved in aggregation of the otolith seed particle and positioning and shaping of the otolith (Colantonio et al., 2009; Wu, Freund, Fraser, & Vermot, 2011; Yu, Lau, Ng, & Roy, 2011). Lack of tether cells leads to a fusion of otoliths that is usually positioned in the middle of the otic vesicle (Millimaki, Sweet, Dhason, & Riley, 2007).

Many ion channels in the membranes of otic epithelial cells help to pump ions and other components into the otic lumen to create and maintain a steady-state of endolymph (Trune, 2010), which is crucial for otolith formation (Blasiole et al., 2006; Ellertsdottir et al., 2006; Lowery & Sive, 2005). In addition, the tight junctions are reported to contribute to the integrity and barrier functions of otic epithelial cells (Tsukita, Furuse, & Itoh, 2001). The tight junctions are intercellular adhesion complexes formed by the close contact between adjacent cells and are often present in the apical region of the epithelial cells (Spring, 1998). Tight junctions act as a semi-permeable barrier to restrain the paracellular transport of ions, solutes and water, and establish a fence to divide the cell membranes into apical and basolateral domains (Anderson & Cereijido, 2001; Dejana, 2004). Occludins, claudins and other junction adhesion molecules are normally associated with the tight junctions (Schneeberger & Lynch, 2004).

Claudins are 18- to 27-KDa integral four-span membrane molecules with two extracellular loops and short N- and C-terminal cytoplasmic domains (Furuse, Fujita, Hiiragi, Fujimoto, & Tsukita, 1998). As claudins are the primary component of tight junctions to form the backbone of tight junction strands, defects of some claudin genes are reported to cause deafness. For instance, mammalian *cldn14* is expressed in the hair cells of cochlea at postnatal day four, and its mutation causes autosomal recessive deafness (Wilcox et al., 2001). A mutation in the zebrafish *cldnj* results in abnormal otolith formation, and hearing and vestibular defects (Hardison, Lichten, Banerjee-Basu, Becker, & Burgess, 2005). *Cldn7*-KO mouse dies within 12 days after birth due to its failure of maintaining epithelial cell–matrix interactions and intestinal homeostasis (Ding et al., 2012), and cldn7 is essential for NaCl homeostasis in distal nephrons (Trune, 2010). However, whether human or mouse cldn7 plays a role in inner ear development has not been studied.

In zebrafish, Cldn7b has been reported as tight-junction molecule in the cells that form epidermal cell aggregates in the ventral jaw region and in the fin-fold. Although *cldn7b* expressed in oitc region was well known, Zebrafish Cldn7 function in inner ear remains to be characterized. In a Tol2 transposon-mediated mutagenesis screen for zebrafish embryonic and developmental defects, we have identified a mutant that carries a Tol2-transposon in its *cldn7b* locus and found that *cldn7b* is expressed in the developing inner ear and the homozygous *cldn7b* mutant exerts noticeable otic defects. The present study thus aims to understand how zebrafish Cldn7b participates in the otic development.

2 | MATERIALS AND METHODS

2.1 | Zebrafish maintenance and mutagenesis

Zebrafish AB line used in this study was obtained from the China Zebrafish Resource Center. Fish maintenance and embryo collection/culture were carried out according to the standard protocols (Westerfield, 2000). Fish embryos were staged according to their morphological features or simply by hpf (Cheung, Webb, Meng, & Miller, 2006). About 50 pg of pGBT-RP2.1(RP2) plasmid DNA and 100 pg of Tol2 transposase mRNA were injected into fertilized eggs at one-cell stage to trap endogenous genes, because it was reported that the expression of trapped genes by RP2 plasmid could be less than 3% of its normal expression level in a tissue- and cell-specific manner (Clark et al., 2011). The *cldn7b* mutant, first identified by the mRFP-expressing embryos, was maintained by crossing its heterozygote with wild-type fish to avoid inbreeding depression.

2.2 | Splinkerette PCR assays and genotyping

Splinkerette PCR assays were performed to obtain sequence information surrounding each Tol2 transposon insertion site (Uren et al., 2009). The $mRFP^+$ F1 were individually outcrossed with wide-type fish to obtain F2 fish, and individual fish genomic DNA was subjected to PCR cloning. *Sau3*AI restricted genomic DNA and a linker were ligated to generate PCR templates. Tol2 R-ITR-specific primers were R1 and R2 and Tol2 L-ITR-specific primers were L1 and L2. Primary PCR was performed with primers pairs Splink1/R1 and Splink1/L1 under the following conditions: 1 cycle at 95°C for 1 min; 10 cycles at 95°C for 10 s, and 70°C for 2 min, decrease 0.5°C/cycle; 20 cycles at 95°C for 10 s and 65°C for 2 min; 1 cycle at 70°C for 10 min. The first-round PCR products were diluted for the nest-PCR assays with primers pairs Splink2/R2 and Splink2/L2 under the following conditions: 1 cycle at 95°C for 2 min; 30 cycles at 95°C for 20 s, 61°C for 30 s and 72°C for 2 min; 1 cycle at 72°C for 10 min. The nested-PCR products were purified through 1.5% agarose gel and cloned into pZero2/TA vector for sequencing. The sequences of PCR products were mapped to the zebrafish genome of ENSEMBL and NCBI database.

The transposon integration of *cldn7b* locus was confirmed by following PCR condition: 95°C for 5 min; 34 cycles at 95°C for 30 s, 58°C for 30 s and 72°C for 30 s; 72°C for 10 min, using three *cldn7b*-specific primers f2, r1, and r2. The linker was obtained by annealing the following Long and Short primers (5′–3′): Long–strand, CGAAGAGTAACCGTTGCTAGGAGAGACCGTGGCTGAATGAG ACTGGTGTCGACACTAGTGG; Short–strand, GATCCCACTAGTGTC-GACACCAGTCTCTAATTTTTTTTTTCAAAAAAA.

Sequences of other primers were:

Splink1, 5′-CGAAGAGTAACCGTTGCTAGGAGAGACC-3′;
Splink2, 5′-GTGGCTGAATGAGACTGGTGTCGAC-3′;
L1, 5′-GATTTTTAATTGTACTCAAGTAAAGTAAAAATCCCC-3′;
L2, 5′-CAGTAATCAAGTAAAATTACTCAAGTACTTTACACC-3′;
R1, 5′-GTACAATTTTAATGGAGTACTTTTTTACTTTTACTCAAG-3′;
R2, 5′-CCAGATACTTTTACTTTTAATTGAGTAAAATTTTCC-3′;
f2, 5′-CGATCTGTCCTTCAGGAATGTGC-3′;
r1, 5′-TTCCATCAATCTCGGATGCTGG-3′;
r2, 5′-TGGAGCCGTACTGGAACTGA-3′.

2.3 | RT-PCR and quantitative real-time PCR (qPCR)

Total RNA was prepared from fish embryos using TRIZOL (Invitrogen, Carlsbad CA), treated with RNase-free DNase at 37°C for 30 min and RNase-inactivated at 65°C for 10 min. The first-strand cDNA was synthesized via First Strand cDNA Synthesis Kit (Fermentas, EU, Lithuania).

RT-PCR was performed as previously described (Song et al., 2012), using primer pairs f1/r2. The PCR products were purified through 1% agarose gel and subjected to sequencing.

The real-time PCR was performed as previously described (Liu et al., 2015) using primer pairs of cldn7bE1F1/cldn7bE2R1 and β-actin-F/β-actin-R (reference pairs), and relative expression of *cldn7b* was calculated by the 2−(ΔΔ Ct) method (Livak & Schmittgen, 2001).

Sequences of primers used were:

f1, 5′-GAGAAGATGGCACATAAAGGACTGC-3′;

r2, 5′-TGGAGCCGTACTGGAACTGA-3′;

cldn7bE1F1, 5′-GCCTTTGGATGTCGTGCGCT-3′;

cldn7bE2R1, 5′- GCCACACCCAGTCCAGCTACTG-3′.

2.4 | Micro-injection

Capped *cldn7b*-mRNA was synthesized through mMESSAGE mMACHINE kit (Ambion, Austin, TX) and each embryo received 300 pg of mRNA that was injected at one-cell stage.

Morpholino oligo (MO), 5′−ACTGAACGCCCGAGTTTGCCATTTC-3′ (Gene Tools Inc., Philomath, OR) against *cldn7a* was injected into one-cell stage fertilized eggs at the indicated doses.

2.5 | Whole-mount RNA in situ hybridization

Whole-mount RNA in situ hybridization (WISH) was carried out as previously described (Thisse C & Thisse B, 2008). Digoxigenin-UTP labeled antisense RNA probes were *cldn7b*, *atp1b2b*, *cldna*, *cldnb*, and *cldnj* (Roche, Mannheim, Germany). Images were taken by a SteReo Lumar V12 microscope (Carl Zeiss, Germany).

2.6 | Immuno-fluorescence staining

24hpf zebrafish embryos were fixed with 4% PFA at 4°C overnight, dehydrated in a gradient of anhydrous methanol (25% and 50%) and kept in 75% of anhydrous methanol at 4°C. The fixed embryos were rehydrated in a gradient of anhydrous methanol (50% and 25%), washed for three times (5 min/time) with PBS containing 0.1% Triton

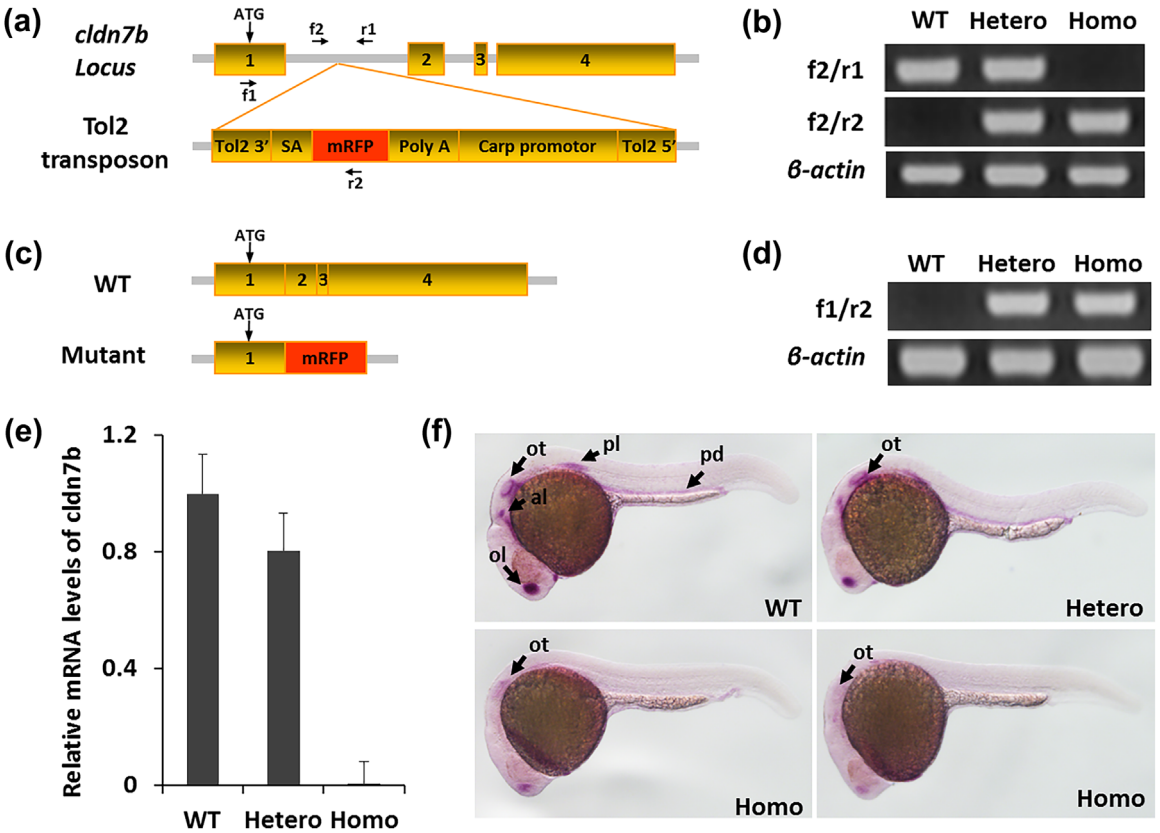

FIGURE 1 The expression of *cldn7b* gene is effectively blocked in the gene-trapping line. a, The genomic locus of zebrafish *cldn7b* gene. Tol2 transposon element was inserted into its first intron. b, PCR primer pairs including f2/r1 and f2/r2 in a, were used for identification of heterozygous (Hetero) and homozygous (Homo) embryos. Wild-type fish (WT) and the β-actin gene were used as controls. c, The *cldn7b*-transcript in WT fish and the predicted cldn7b-mRFP fusion transcript in mutants. d, RT-PCR analysis confirms the presence of *cldn7b*-mRFP fusion transcripts. Primers used are indicated in a, β-actin was used as positive control. e, Real-time qPCR analysis of *cldn7b* transcription expression in WT, heterozygous, and homozygous embryos at 24hpf. The expression of β-actin gene was used as an internal control. Error bars: standard deviation. f, WISH assays revealed the expression of *cldn7b* in WT, heterozygous, and homozygous embryos at 24hpf. ol, olfactory placode; ot, otic vesicle; al, anterior lateral line primordium; pl, posterior lateral line primordium; pd, pronephric duct

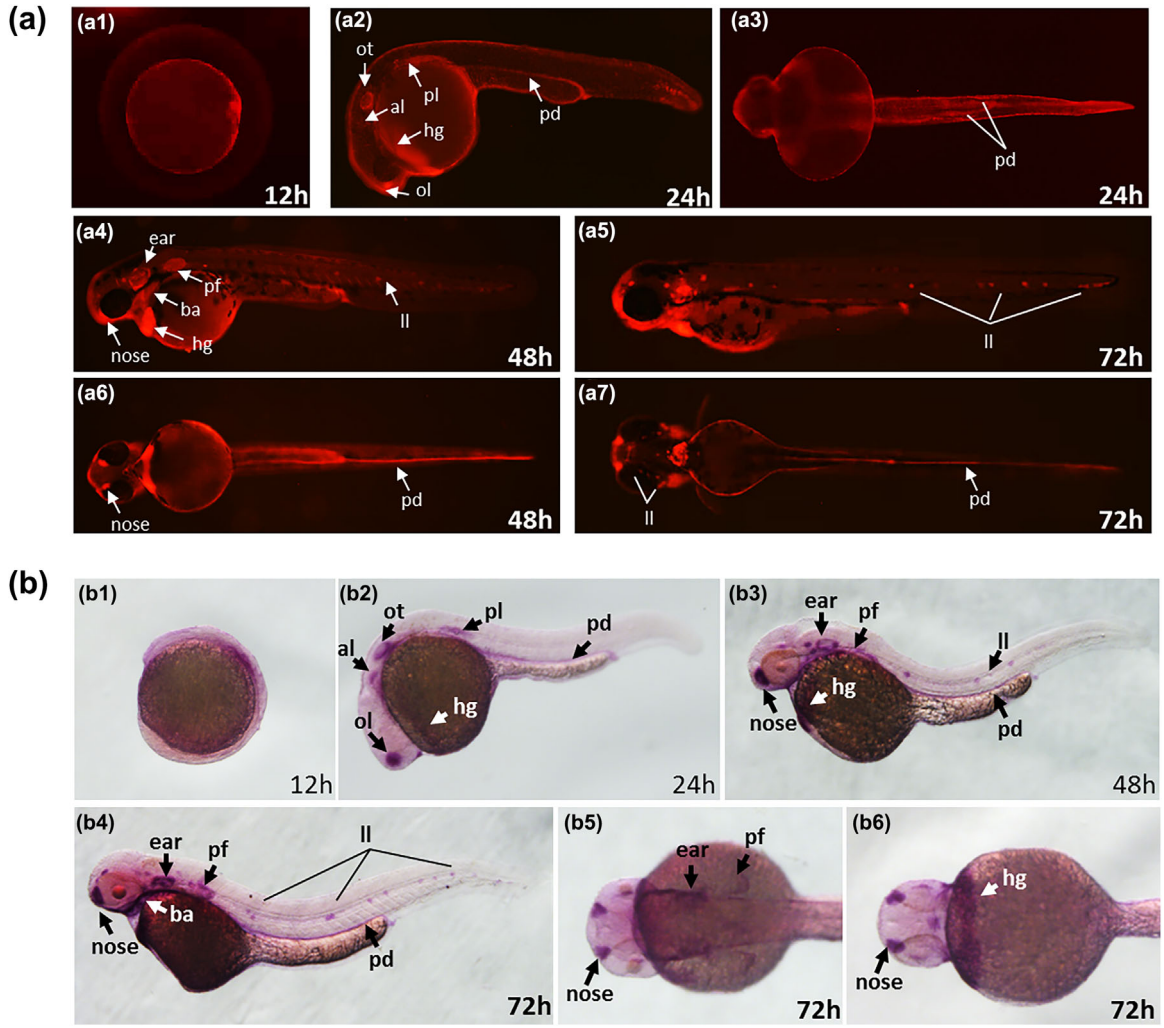

FIGURE 2 Expression patterns of *cldn7b*-mRFP are similar to those of endogenous *cldn7b* gene. a, Cldn7b-mRFP expression patterns in heterozygous *cldn7b*-mutant embryos. a2, a4 and a5 lateral views; a3, a6 and a7 ventral view. b, WISH assays revealed the expression of *cldn7b* in heterozygous *cldn7b*-mutant embryos. b2, b3 and b4 lateral views; b5 dorsal view; b6 ventral view; al, anterior lateral line primordium; ba, branchial arches; hg, hatching gland; ll, lateral line neuromast; ol, olfactory placode; ot, otic vesicle; pd, pronephric duct; pf, pectoral fin; pl, posterior lateral line primordium

and blocked with PBS containing 10% goat serum for 1 hr at room temperature. Pre-blocked Embryos were incubated with the acetylated α-Tubulin antibody (1:500, Sigma, St. Louis, Sigma, St. Louis, MO) over night at 4°C, washed with PBS containing 0.1% Triton for six times (20 min/time) and incubated with FITC-conjugated secondary antibody (anti-mouse IgG, 1:50, BOSYER, Wuhan, China) over night at 4°C. After extensive wash (PBS containing 0.1% Triton, 6 × 20 min), and incubation with DAPI, embryos were imaged with a confocal microscope (Leica SP8, Germany).

2.7 | C-start escape behavior test

Sound-evoked C-start escape behavior experiments were performed and scored as previously described (Han et al., 2011). Successful C-Start was identified manually as described previously (Mu, Li, Zhang, & Du, 2012).

2.8 | Transmission electronic microscopy and histology

Embryos were fixed with PBS buffer (pH 7.4) containing 2.5% glutaraldehyde and 1% OsO4, dehydrated with graded ethanol and acetone, and infiltrated and embedded with Spurr's epoxy resin. Series of ultra-thin sections (70 nM) were double stained with 2% uranyl acetate and Sato's lead citrate and imaged through a transmission electron microscope. Histological sections (1.5 μM) were stained with 1% toluidine blue and imaged.

2.9 | Measurement and statistics

The areas of otic lumens and size of otolith of fish embryos or larvae were obtained by measuring their longest and shortest diameters under a microscope and using the averaged diameter of each lumen or otolith to

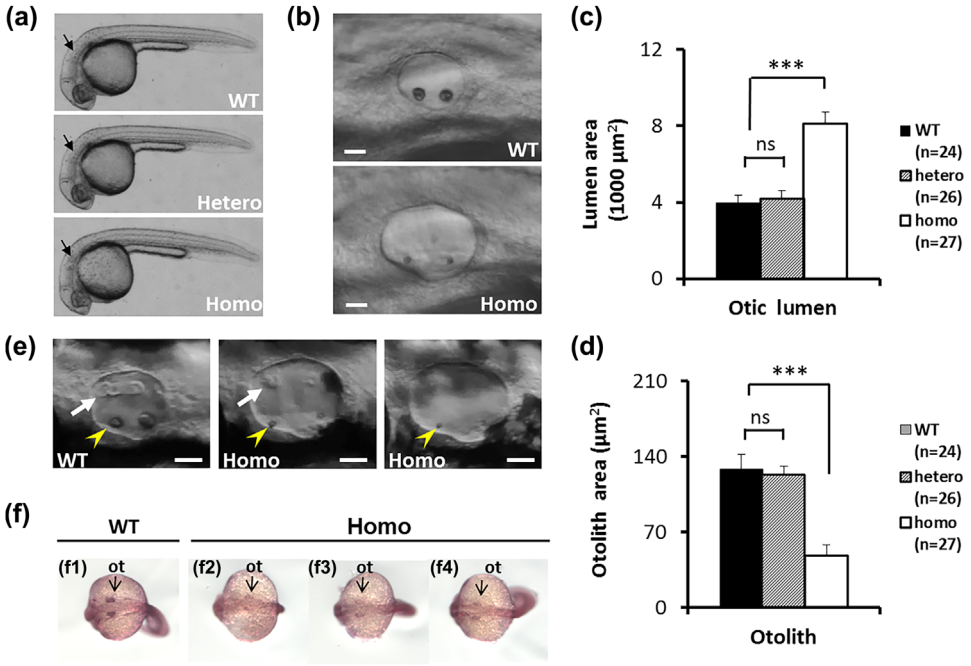

FIGURE 3 The defects in the inner ear of homozygous *cldn7b*-mutants. a, Morphological phenotypes of wild-type (WT), heterozygous (Hetero), and homozygous (Homo) embryos at 24hpf. Otic vesicle(OT) is indicated in black arrow. b, The morphology of OT in WT and homozygous embryos at 24hpf. Scale bars: 30 mm. c,d, Statistical analysis of the otic lumen area and otolith area in different types of embryos at 30hpf. Individuals of WT and homozygous embryos were randomly selected for statistical analysis of otic lumen and otolith areas at 30hpf. The otic lumen and otolith areas were measured in the focal plane representing the maximal area. ns, non-significant; ***, $p < 0.0001$. e, OT of WT and homozygous embryos at 60hpf showing the semicircular canal protrusions (white arrow) and otoliths (yellow arrowhead). Scale bars: 10 mm. f, WISH assays revealed the expression of *cldn7b* in OT of wild-type and homozygous embryos at 24hpf

determine its area ($S = \pi ab$). Student's *t*-test was used to determine the statistical difference of (at least $p < 0.05$) control and experimental groups.

3 | RESULTS

3.1 | Identification of a *cldn7b* mutant

In a mutagenesis screen of Tol2 gene-trapping lines, we identified a zebrafish line carrying the Tol2-trapping cassette inserted in first intron of *cldn7b* (Figure 1a), the *cldn7b*-trapping fish. Using two primer pairs, that is, f2/r1 and f2/r2, heterozygotes and homozygotes of *cldn7b*-trapping fish could be distinguished by PCR assays (Figure 1b). Both mature heterozygotes and homozygotes of *cldn7b*-trapping fish were present in individuals from in-cross of the heterozygous trapping fish. By their RFP fluorescence intensity, we could also distinguish heterozygotes from homozygotes of *cldn7b*-trapping fish. Out of total 1,568 embryos obtained from in-crosses of *cldn7b*-trapping fish, 25.8% had no RFP, 50.9% showed moderate RFP and 23.3% exerted strong RFP, consistent to genotyping RT-PCR (Supplementary Figure S1). These results suggested that heterozygous *cldn7b*-trapping fish should contain a single transposon insertion and pass the insertion to next generation in a Mendelian fashion.

Due to the transposon insertion that provided a splicing acceptance site at 5′ end of mRFP coding region, a fusion protein containing N-terminal 74 amino acid residues of Claudin7b and mRFP (Figure 1c) was predicted in *cldn7b*-trapping fish. Indeed, by reverse transcription-PCR (RT-PCR) using primer pair f1/r2, a DNA fragment derived from alternative splicing of transposon-inserted *cldn7b* locus could be detected in both heterozygotes and homozygotes of *cldn7b*-trapping fish but not in wild-type fish (Figures 1c and 1d). Real-time quantitative PCR (qPCR) analysis indicated that *cldn7b* expression level was slightly decreased by ~20% in heterozygotes and drastically reduced by ~99% in homozygotes of *cldn7b*-trapping fish at 24hpf (Figure 1e). WISH assay also indicated a slight reduction of *cldn7b* transcription level in heterozygous embryos of *cldn7b*-trapping fish, while in homozygotes, *cldn7b* transcripts were either barely detectable or absent at 24hpf (Figure 1f). Therefore, at 24hpf, homozygous *cldn7b*-trapping fish is a loss-of-function mutant with incomplete penetrance.

3.2 | Expression pattern of *cldn7b*

Taking advantage of the "knock-in" mRFP coding sequence in *cldn7b* mutant, we could monitor RFP fluorescence of heterozygous mutant. Fluorescent signal was first visible in the epidermis at 12hpf and specifically in the hatching glands, pronephric ducts, olfactory placodes, and otic vesicles, and lateral line primordia at 24hpf. At 48 and 72hpf, mRFP was also observed in the pectoral fins and branchial arches, in addition to the hatching glands, pronephric ducts and some peripheral sensory organs (Figure 2a). WISH assays indicated that the endogenous *cldn7b* expression pattern was similar to that of Cldn7b-mRFP at same developmental stages (Figure 2b).

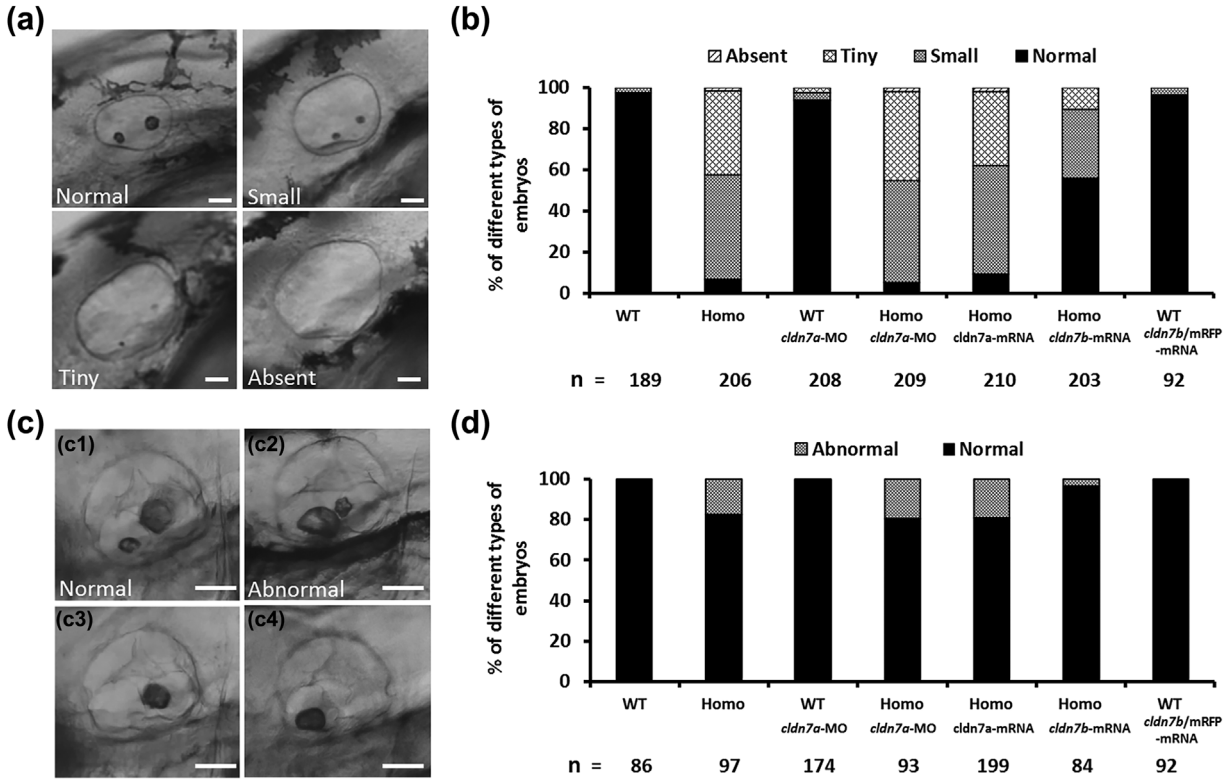

FIGURE 4 The variable otolith sizes and rescuing effects of *cldn7b*-overexpression in mutants. a, The variable otolith sizes of homozygous *cldn7b*-mutant embryos at 36hpf. According to the otolith sizes, mutant embryos were classified into four groups: normal, small, tiny, and absent. Scale bars: 30 mm. b, Percentages of embryos in each group at 36 hr. Embryos at one-cell stage were injected with *cldn7a*-morpholino (10 ng/embryo) or capped mRNA (300 pg/embryo). WT, wild-type; Homo, homozygous embryos; WT clan7a-MO, wild-type embryos injected with *cldn7a*-morpholino; Homo *clan7a*-MO, homozygous embryos injected with *cldn7a*-morpholino; Homo *cldn7a*-mRNA, homozygous embryos injected with capped *cldn7a*-mRNA; Homo *cldn7b*-mRNA, homozygous embryos injected with capped *cldn7b*-mRNA; WT *cldn7b*/mRFP-mRNA: wild-type embryos injected with *cldn7b*/mRFP capped mRNA. *n*, the number of observed embryos. c, The phenotypes of fused otoliths in homozygous *cldn7b*-mutant embryos at 5 dpf. a, normal otolith in wild-type; b–d, abnormal otolith in *cldn7b*-mutants. Otoliths fused partly in b and totally in c and d. Fish Head points to the front. Scale bars: 6 mm. d, Percentages of embryos in each group at 5 dpf. Embryos at one-cell stage were injected with *cldn7a*-MO (10 ng/embryo) or corresponding capped mRNA (300 pg/embryo). WT, wild-type; Homo, homozygous embryos; WT *clan7a*-MO, wild-type injected with *cldn7a*-MO; Homo *clan7a*-MO, homozygous embryos injected with *cldn7a*-MO; Homo *cldn7a*-mRNA, homozygous embryos injected with capped *cldn7a* mRNA; Homo *cldn7b*-mRNA, homozygous embryos injected with capped *cldn7b* mRNA; WT *cldn7b*/mRFP-mRNA: wild-type injected with capped *cldn7b*/mRFP mRNA. *n*, the number of observed embryos

Cldn7b-mRFP fusion protein retained only the first transmembrane domain including 5–27 amino acid residues of Cldn7b (Supplementary Figure S2), so this domain appears to be critical for the normal localization of Cldn7b to specific tissues and cells in zebrafish.

As homozygous *cldn7b* mutants were viable and fertile, we examined if homozygous mutants had specific non-lethal defects. To examine specific morphological defects of the homozygous mutant embryos, we focused on *cldn7b*-expressing organs and observed that homozygous mutants developed larger otic otocysts and smaller otoliths at 24hpf, compared to those of wild-type embryos (Figures 3a and 3b). At 30hpf, both otic vesicle lumen areas and otolith sizes of wild-type and mutant embryos were measured and compared, the results further supported the otic defect of homozygous mutants (Figures 3c and 3d). At 50hpf, wild-type larvae already developed the semicircular canals, whereas some homozygous mutants failed to grow epithelia protrusions into the otic lumen or just began to outgrow the protrusions (Figure 3e). WISH assays also showed that *cldn7b* is barely expressed in homozygous mutant otic area (Figure 3f), indicating a correlation between the otic defects and extremely low level of *cldn7b* expression or the presence of Cldn7b-mRFP fusion protein in mutant otic vesicles.

3.3 | Loss of *Cldn7b* function results in otic defects

Variable otic defects of homozygous *cldn7b* mutants, represented by four otolith phenotypes, that is, at 36hpf, normal (comparable to that of wild-type), small (35–75% of normal), tiny (5–34% of normal), and absent (less than 5% of normal) groups (Figure 4a), supported the idea that the homozygous mutant phenotypes were not fully penetrated. Less than 2% of otic vesicles ($n = 189$) in wild-type embryos could be categorized into small group, while over 95% of homozygous mutant otic vesicles ($n = 206$) had tiny, small or no otolith (Figure 4b). These

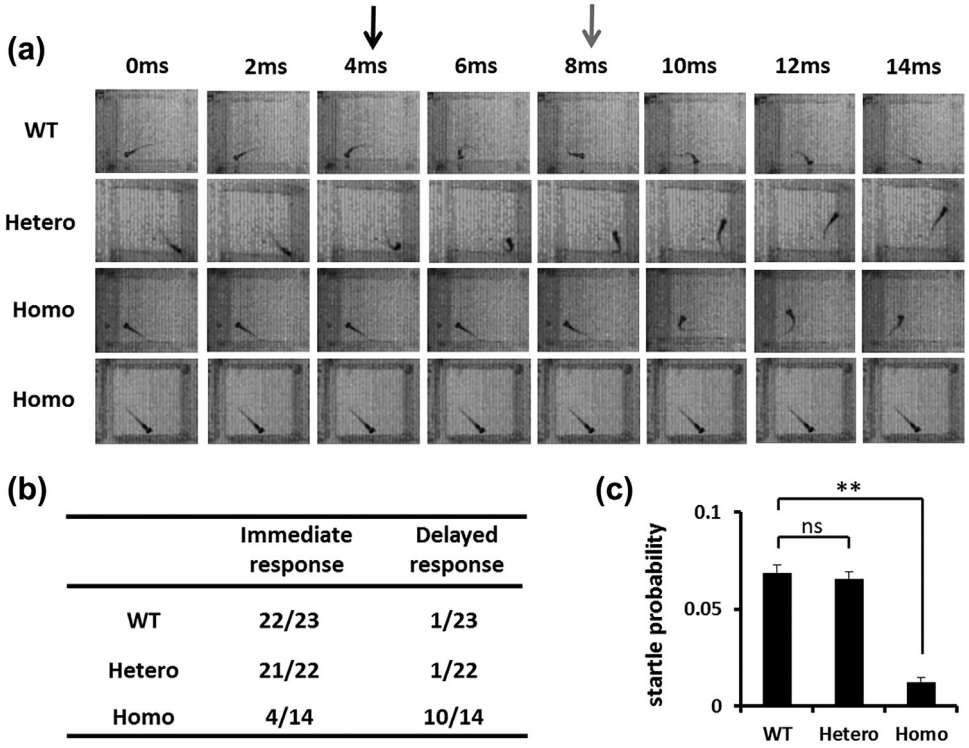

FIGURE 5 Hearing disability of homozygous *cldn7b*-mutants at 5 dpf. a, C-Start escape response of embryos in different genotypes to the sound stimuli at 500-Hz frequency and 10 ms duration. The successful C-Start escape response was initiated within 4 ms after the sound stimulation. b, Statistical data showed the proportion of immediate and delayed responses in three genotypes. Data represent the number of immediate response or delayed response versus number of total response. c, The average probability of C-start escape response. The probability was calculated by including the successful C-Start escape response. For each group, 32 larvae were tested. ns, non-significant; $**$, $p < 0.001$

observations suggested that functional redundancy of Cldn7b and Cldn7a that share 71% amino acids might contribute to variable otic defects in homozygous *cldn7b* mutants. However, only knocking down *cldn7b* but not *cldn7a* in wild-type embryos could lead to variable otolith phenotypes of ears (data not shown), while only injecting *cldn7b* but not *cldn7a* mRNA could partially restore normal otolith development in homozygous mutant otic vesicles, from 6.4 to 55.7% (Figure 4b).

To see if MO-mediated *cldn7a* knockdown in fact targeted endogenous *cldn7a*, we co-injected *cldn7a*-MO or standard control MO and an indicator plasmid, which bears *cldn7a*-MO recognition site in front of the GFP coding region, into one-cell stage embryos. Only *cldn7a*-MO could abolish GFP signal (Figures S3a and S3b). On the other hand, injecting *cldn7a*-mRNA failed to rescue homozygous *cldn7b* mutant phenotypes, apparently not due to insufficient amount of Cldn7a present in injected homozygous mutant embryos because HA-tagged Cldn7a was abundantly enriched in the injected embryos (Supplementary Figure S3c). Therefore, Cldn7a did not contribute to otic development.

Because of the normal ear development in heterozygous *cldn7b* mutant embryos (Figure 1), we predicted that otic defects of homozygous mutants were not due to the presence of Cldn7b-mRFP fusion protein. To confirm this notion, in vitro synthesized capped *cldn7b/mRFP*-mRNA was injected into wild-type embryos yet the otolith formation was not affected (Figures 4b and 4d), suggesting that Cldn7b-mRFP fusion protein did not interfere with normal function of Cldn7b. Therefore, low level of *cldn7b* expression appeared to singly lead to otic defects in homozygous *cldn7b* mutants.

The facts that otic vesicle sizes of wild-type and homozygous *cldn7b* mutant were comparable; only 17.5% homozygous mutants had two otoliths ($n = 97$) that almost fused, or one big otolith, compared to wild-type otic vesicles that contained an utricle (small) otolith and a saccular otolith (large) (Hughes, Thalmann, Thalmann, & Ornitz, 2006), and the semicircular canals were also present in homozygous mutant ears (Figure 4c), indicated that the otic defects were somewhat recovered at 5 dpf in homozygous mutant larvae. At this stage, percentage of abnormal otolith ears could be reduced, from 17.5 to 3.5%, only by introduction of *cldn7b* mRNA. Neither *cldn7a* nor *cldn7b-mRFP* could change the otolith phenotype (Figure 4d), also supporting the prediction that low *cldn7b* expression level is responsible for the embryonic defects of otic development in homozygous mutants.

To see if the observed embryonic ear defects affected ear function of homozygous mutant larvae, C-startle response experiment was performed (Baxendale, Whitfield, Romand, & Varela-Nieto, 2014). At 5 dpf, wild-type and heterozygous mutant larvae could immediately respond to near-field pure tone stimulation within 4 ms, but homozygous mutant larvae either had a delayed response at 8 ms or no response at all (Figure 5a). The proportion of immediate response

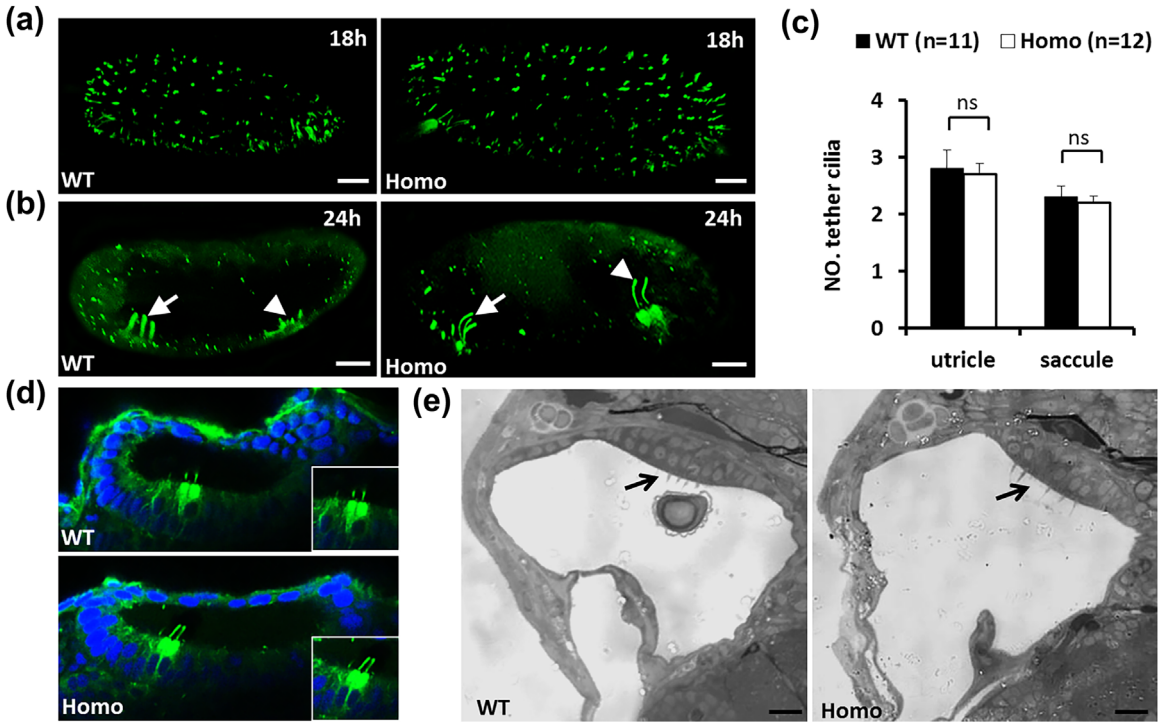

FIGURE 6 Deficiency of *cldn7b* expression does not affect the hair cell development. a, Acetylated tubulin staining in wild-type (WT) and homozygous (Homo) embryos at 18hpf showed the short cilia within the otic vesicle. Scale bars, 10 μM. b, Acetylated tubulin staining in wild-type and homozygous embryos at 24hpf showed two clusters of long tether cilia. Arrow: long tether cilia in the utricular maculae; arrowhead: long tether cilia in the saccular maculae. Scale bars, 10 μM. c, Statistical analysis of long tether cilia numbers in the utricular and saccular maculae of embryos at 24hpf. ns, non-significant. d, Acetylated tubulin staining revealed the location of hair cells in utricle maculae. Right corner represents an enlarged area. e, Histology sections of inner ear in wild-type and homozygous embryos at 5 pdf. Black arrow indicates the hair cell bundle. Scale bars, 50 μM. We sectioned wild-type and homozygous in the same angles by cutting the embryos perpendicular to dorsal ventral axis

and delayed response for three genotypes were shown in Figure 5b. As described previously (Baxendale et al., 2014), the successful C-startle was identified excluding delayed response, so the probability of C-startle response for wild-type and heterozygous larvae was indistinguishable and significantly higher than that of homozygous mutants (Figure 5c). Overall, the averaged C-startle response time of homozygous mutant larvae was significantly increased, compared to that of wild-type and heterozygous larvae, consistent to notion that low *cldn7b* expression level accounted for otic defects in developing homozygous mutant ears.

3.4 | Homozygous *cldn7b* mutant has normal mechanosensory hair cells

Inner ear hair cells are responsible for converting vibration sensation or mechanical stress to electrical/chemical signals that initiate auditory or vestibular circuitry (Baxendale et al., 2014). Although majority (~80%) of homozygous *cldn7b* mutant larvae showed normal otolith number and semicircular canals in the ear at 5 dpf (Figures 4c and 4d), suggesting a recovery from early abnormal otic development, some homozygous mutants exerted delayed C-startle response (Figure 5) might point out the possibility that early development of hair cells was affected in the homozygous mutant ears. To this end, we examined whether the number and morphology of hair cells were normal in the homozygous mutant ears. Acetylated-tubulin antibody stained short cilia of all otic cells at 18hpf (Figure 6a) and kinocilia of the tether cells at 24hpf (Figure 6b). Each mature hair cell grows only one kinocilia, so the number of kinocilia thus represents the number of hair cells. We found that both wild-type and homozygous mutant developed same number of hair cells in their utricle and saccule (Figure 6c). WISH assay using a hair cell-specific marker gene, *atp1b2b* (Roberts, Elsner, & Bagnall, 2017), also revealed that *atp1b2b* expression pattern was not changed in the homozygous mutant ears (Supplementary Figure S4). Using both acetylated-tubulin antibody and DAPI to stain otic cells, the location and shape of utricular hair cells were indistinguishable between wild-type and homozygous mutant ears at 24hpf (Figure 6d). By 5 dpf, histological sections of otocysts of wild-type and homozygous mutant at the same positions also revealed that a row of hair cells and underneath support cells were neatly arranged in their maculae, with or without otoliths (Figure 6e). Therefore, the development of hair cells appeared normal in homozygous mutant otocysts, although the misplacement or a lack of otolith in homozygous mutant ears could still be responsible for C-startle response defect of some but not all homozygous mutants at 5 dpf (Figure 5b).

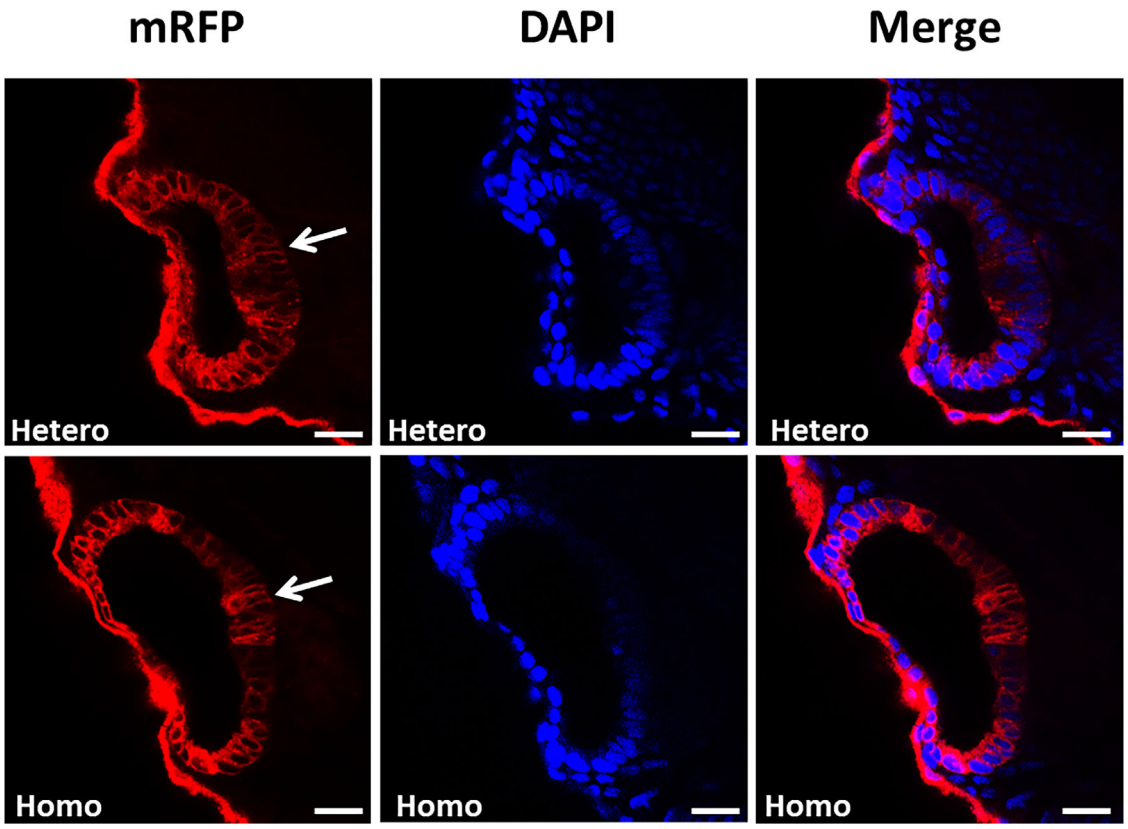

FIGURE 7 Subcellular localization of *cldn7b*-mRFP fusion proteins. *Cldn7b*-mRFP fusion proteins were located in the membrane of otic epithelial cells in heterozygous mutants at 24 dpf. The layer of otic epithelial cells in homozygous mutants is thinner than that in heterozygous mutants. The arrow points to the thinner regions with anterior to the top and dorsal to the left. Scale bars, 40 μM

3.5 | Low *Cldn7b* level leads to malformation of tight junctions in homozygous mutant otic epithelia

The presence of Cldn7b-mRFP fusion protein in heterozygous and homozygous mutant ears allowed us to closely examine where truncated Cldn7b with only single transmembrane domain was located. In the otic vesicles of heterozygous and homozygous mutant embryos at 24hpf, Cldn7b-mRFP was present at the membrane of all otic cells but not in their nuclei (Figure 7). Perhaps due to a larger otic lumen of homozygous mutants, ventral otic epithelium was thinner than that of heterozygous mutants (Figure 7), likely correlating to otic developmental delay.

Many claudin-encoding genes such as *cldna*, *cldnb*, and *cldnj* and the epithelial cell adhesion molecule *epcam* were also expressed indistinguishably in developing ears of both wild-type and homozygous mutant ears at 24hpf (Figure 8a). It is possible that multiple claudins including Cldn7b are all needed and fine arranged to allow tight junction strands of otic epithelia to tightly seal the otic vesicle during ear development. In this sense, low *cldn7b* expression level in homozygous mutant otic cells might lead to delayed otic development during embryogenesis (24hpf) and some defects of mutant ear function (5 dpf). Indeed, the integrity of apical junction complexes (AJCs) of homozygous mutant ears was less profound than that of wild-type ears at 36hpf, 60hpf, and 5 dpf, because the length of otic epithelial AJCs was shorter than that of wild-type AJCs (Figure 8b-c; Supplementary Figure S5). Furthermore, the defect of otic epithelial AJCs was largely rescued in *cldn7b*-mRNA injected homozygous mutants at 36hpf and 60hpf (Supplementary Figure S5). Therefore, low *cldn7b* expression level is likely responsible for otic defects in developing homozygous mutant ears.

Based on the results of this study, functions of Cldn7b in the inner ear were outlined in Figure 8d. The insertion of Tol2 transposon disrupted the expression of the *cldn7b* gene and the loss of claudin7b damages the formation and integrity of AJCs in the otic epithelium. Damaged AJCs in the otic epithelium of homozygous *cldn7b*-mutants fail to provide the appropriate ion conditions required for the formation of otoliths and vestibular canals, which are essential for the hearing of inner ear in zebrafish.

4 | DISCUSSION

In this study, we have characterized a zebrafish *cldn7b* mutant and revealed specific ear defects including enlarged otocysts, small or no otoliths, delayed formation of semicircular canals and abnormal AJCs of otic epithelia during embryogenesis. We have demonstrated that the developmental ear defects are largely due to a loss-of-*cldn7b* expression in the homozygous mutants. Most otic defects, except the

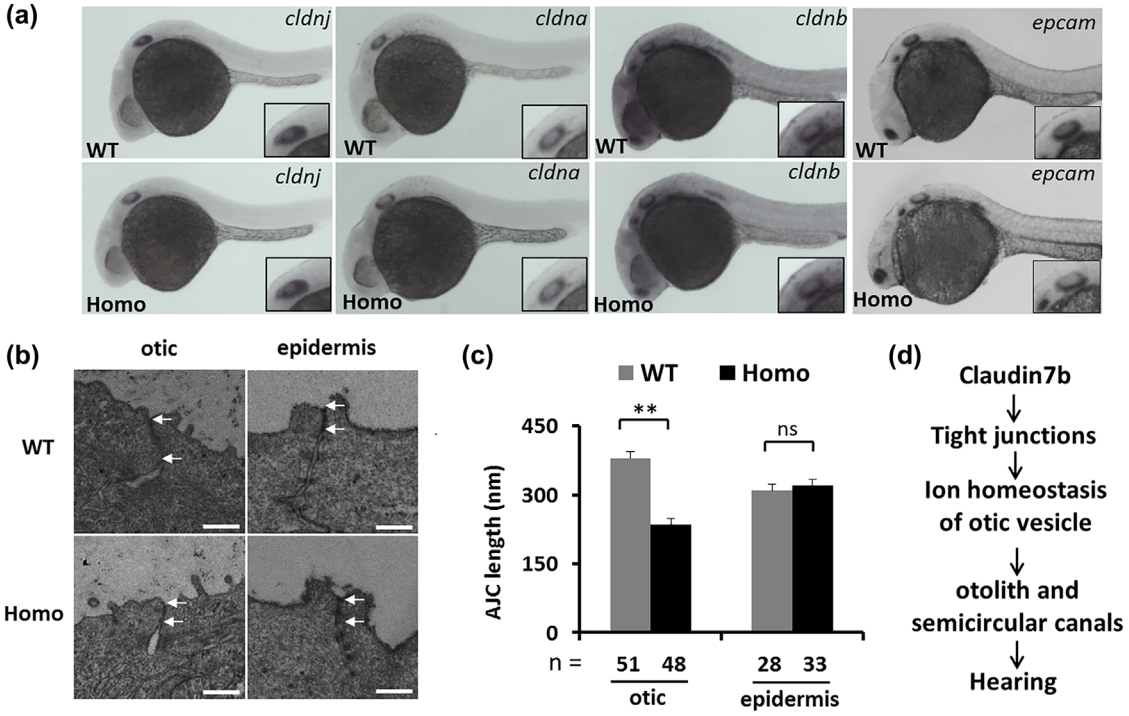

FIGURE 8 Tight junctions among otic epithelial cells. a, Whole-mount in situ hybridization (WISH) revealed a similar expression patterns of the claudin family genes *cldna*, *cldnb*, and *cldnj*, and the epithelial cell adhesion molecule epcam in wild-type and homozygous mutants and the expression of *cldna*, *cldnb*, *cldnj*, and *epcam* appeared to be normal in homozygous mutants at 24hpf. b, Apical junction complexes (AJCs) within otic epithelial and epidermal were revealed by transmission electronic microscope. The length of AJCs between two adjacent cells was marked by the pace between two arrows. Five embryos of wild-type (WT) and five homozygous (Homo) mutant at 5 dpf were examined. Scale bars: 200 nM. c, The statistical data of average AJCs length. *n*, total number of the AJCs; ns, non-specific. $**$, $p < 0.001$. d, A working model to show functions of *Cldn7b* in inner ear of zebrafish.

AJCs phenotype of homozygous mutant larval ears, are self-recovered to some extent in late developmental stages, perhaps due to redundant functions of or compensation from other claudins that are also expressed in otic epithelia. However, some homozygous mutant larvae fail to properly respond to sound stimulation. The present study thus unveils an important and unique role of Cldn7b played during otic development.

Teleost otolith is a stone-like complex in the saccule or utricle of the inner ear, made of concentric layers of organic matrix alternating with $CaCO_3$ (Lundberg et al., 2015). The correct formation of otoliths is essential for optimal ear function. It is roughly a multiple-step process, that is, after initial seeding, otolithic crystallites quickly attach to the tether cell kinocilia and aggregate to rapidly grow during ear development (Stooke-Vaughan, Huang, Hammond, Schier, & Whitfield, 2012). Many otoconial proteins are essential for $CaCO_3$ crystallization because they are able to bind calcium in calcium-poor endolymph. Proteins that are not incorporated into otoliths (non-constituent) also regulate the crystallization process by establishing an appropriate milieu of calcium and other ions ideal for crystal seeding and growth. In concert with channel/pump proteins, enzymes and trafficking molecules (over 70 mutants have been identified to affect otolith formation in zebrafish), local concentrations of Ca^{2+} and HCO_3^- are high enough to form $CaCO_3$ crystallites (Abbas & Whitfield, 2010; Hughes et al., 2006). The third step is maintenance of otolith tethering, that is, continuous addition of both organic and inorganic components and fusion of minute crystallites then ensure proper otolith growth.

Several claudins are studied for their roles in ear development and otic functions. It is known that mutated Cldnj, a tight junction protein, results in zebrafish with smaller otoliths, no response to tapping stimuli and balancing problem. The otolith phenotype is due to dispersed crystal seeding particles or slow aggregation/fusion of crystallites in the otic vesicle of homozygous *cldnj* mutant even at 5 dpf (Hardison et al., 2005). As otic vesicle of homozygous *cldnj* mutant is morphologically normal, that is, normal size and semicircular canal formation, it appears that Cldnj functions to maintain an endolymphic composition by providing a barrier or passage channel of specific ions. The failure of otolith growth in homozygous *cldnj* mutant ear is also possibly due to a loss of interaction of Cldnj and signaling molecules, which is essential for ear function. Interestingly, human Cldn14 mutation causes congenital deafness but ear morphology is normal (Wilcox et al., 2001), although whether patients possess otoconia defect to cause balance problem is yet to be determined. Therefore, losing otic Cldnj might be unrelated to otic epithelia integrity. It is possible that small otoliths in homozygous *cldnj* mutant ears are unable to create a normal shearing force to depress kinocilia of hair cells so that the vestibular circuitry is not fully functioning.

The homozygous *cldn7b* mutant ears exert different developmental defects from those of homozygous *cldnj* mutants, but are reminiscent of otic defects found in homozygous *grhl2* mutants (Han et al., 2011). The homozygous *grhl2* mutants exhibit enlarged otocysts, smaller or eliminated otoliths, malformed semicircular canals, insensitiveness to sound stimulation and imbalanced swimming behavior. However, in homozygous *grhl2* mutants, expression of *cldnb* and *epcam* was severely reduced, and putting back both *cldnb* and *epcam* mRNA can rescue homozygous *grhl2* mutant otic phenotypes. Mutation of *epcam*, encoding an epithelial adhesion molecule, also results in smaller otoliths and slightly enlarged otic vesicles, perhaps due to its indispensable role for the epithelial integrity (Slanchev et al., 2009). In fact, injecting *epcam* or *cldnb* mRNA alone similarly rescues homozygous *grhl2* mutant otolith defect (Han et al., 2011), indicating that the severe otic defects of homozygous *grhl2* mutants are attributed to the loss of *cldnb* and *epcam* functions. It remains unknown if *cldnb* mutant shares otic phenotypes of *epcam* mutant and if Cldnb and Cldnj share any similar role in ear development. There are half dozen claudin genes (*cldn7b*, *cldna*, *cldnb*, *cldnf*, *cldnh*, and *cldnj*) expressed in otic cells during embryogenesis (ZFIN.org). Unlike otic defects of homozygous *cldnj* and *grhl2* mutants, homozygous *cldn7b* mutants seldom show any obvious defect of balancing behavior (data not shown) and gradually recover most of their otic defects. Therefore, a further question is whether other ear-expressed claudins could gradually compensate the early loss of Cldn7b function in homozygous *cldn7b* mutants.

In normal development, the cavitation of otic placode allows polarized otic epithelia, connected with tight junctions and adhesive molecules, to become a well-balanced ionic, fluid-filled vesicle that favors development of sub-organs such as the otoliths and semicircular canals. In this sense, the enlarged otic vesicles of homozygous *cldn7b* and *grhl2* mutants, due to an abnormal ion-homeostasis or "leaky" barrier, unlikely provide an endolymphic environment to support otolith growth and semi-circular canal formation. Otolith seeding and growth are essentially normal in homozygous *cldn7b* mutant ears, indicative of the presence of normal otoconial or non-constituent otolithic proteins. As in homozygous *cldnj* and *grhl2* mutant ears, the otoliths remain small or missing, and in less than 20% homozygous *cldn7b* mutant ears, otoliths are mis-located, yet their hair cells are normally grown in the utricle and saccule, the lack of proper contact between otoliths and hair cells may explain why homozygous *cldnj* and *grhl2* mutants and a few homozygous *cldn7b* mutants exert un-balanced motion. Although the delayed otolith development does not affect zebrafish vestibular circuitry establishment/assembly, the ultimate presence and growth of otoliths are crucial for vestibular sensing (Roberts et al., 2017).

ACKNOWLEDGMENTS

We thank Prof. Jiulin Du and Weiyu Chen at Institute of Neuroscience, Shanghai Institutes for Biological Sciences, Chinese Academy of Sciences, for their technical assistance with the C-start escape behavior tests. We thank Yingla Zhang of Beijing University for her assistance with the revision of the manuscript. This research was supported by grants from the National Natural Science Foundation of China (#31571504 to Z. Cui and # 31571496 to D. Liu) and the National Basic Research Program of China (#2012CB944500).

ORCID

Zongbin Cui http://orcid.org/0000-0002-3443-3168

REFERENCES

Abbas, L., & Whitfield, T. T. (2010). The zebrafish inner ear. *Fish Physiology: Zebrafish*, *29*, 123.

Anderson, J., & Cereijido, M. (2001). Introduction: Evolution of ideas on the tight junction. *Tight junctions* (pp. 1–18). Boca Raton: CRC Press.

Baxendale, S., Whitfield, T. T., Romand, R., & Varela-Nieto, I. (2014). Zebrafish inner ear development and function. *Development of Auditory and Vestibular Systems*, 63–106.

Blasiole, B., Canfield, V. A., Vollrath, M. A., Huss, D., Mohideen, M.-A. P., Dickman, J. D., … Levenson, R. (2006). Separate Na, K-ATPase genes are required for otolith formation and semicircular canal development in zebrafish. *Developmental Biology*, *294*(1), 148–160.

Cheung, C. Y., Webb, S. E., Meng, A., & Miller, A. L. (2006). Transient expression of apoaequorin in zebrafish embryos: Extending the ability to image calcium transients during later stages of development. *International Journal of Developmental Biology*, *50*(6), 561.

Clark, K. J., Balciunas, D., Pogoda, H.-M., Ding, Y., Westcot, S. E., Bedell, V. M., … Petzold, A. M. (2011). In vivo protein trapping produces a functional expression codex of the vertebrate proteome. *Nature methods*, *8*(6), 506–512.

Colantonio, J. R., Vermot, J., Wu, D., Langenbacher, A. D., Fraser, S., Chen, J.-N., & Hill, K. L. (2009). The dynein regulatory complex is required for ciliary motility and otolith biogenesis in the inner ear. *Nature*, *457*(7226), 205–209.

Dejana, E. (2004). Endothelial cell-cell junctions: Happy together. *Nature Reviews Molecular Cell Biology*, *5*(4), 261–270.

Ding, L., Lu, Z., Foreman, O., Tatum, R., Lu, Q., Renegar, R., … Chen, Y. H. (2012). Inflammation and disruption of the mucosal architecture in claudin-7-deficient mice. *Gastroenterology*, *142*(2), 305–315.

Ellertsdottir, E., Ganz, J., Dürr, K., Loges, N., Biemar, F., Seifert, F., … Driever, W. (2006). A mutation in the zebrafish Na, K-ATPase subunit atp1a1a. 1 provides genetic evidence that the sodium potassium pump contributes to left-right asymmetry downstream or in parallel to nodal flow. *Developmental Dynamics*, *235*(7), 1794–1808.

Fritzsch, B., & Beisel, K. (2001). Evolution and development of the vertebrate ear. *Brain Research Bulletin*, *55*(6), 711–721.

Fritzsch, B., Pauley, S., & Beisel, K. W. (2006). Cells, molecules and morphogenesis: The making of the vertebrate ear. *Brain Research*, *1091*(1), 151–171.

Furuse, M., Fujita, K., Hiiragi, T., Fujimoto, K., & Tsukita, S. (1998). Claudin-1 and-2: Novel integral membrane proteins localizing at tight junctions with no sequence similarity to occludin. *The Journal of Cell Biology*, *141*(7), 1539–1550.

Han, Y., Mu, Y., Li, X., Xu, P., Tong, J., Liu, Z., & Meng, A. (2011). Grhl2 deficiency impairs otic development and hearing ability in a zebrafish model of the progressive dominant hearing loss DFNA28. *Human Molecular Genetics*, *20*(16), 3213–3226.

Hardison, A. L., Lichten, L., Banerjee-Basu, S., Becker, T. S., & Burgess, S. M. (2005). The zebrafish gene claudinj is essential for normal ear function and important for the formation of the otoliths. *Mechanisms of Development*, *122*(7), 949–958.

Hughes, I., Thalmann, I., Thalmann, R., & Ornitz, D. M. (2006). Mixing model systems: Using zebrafish and mouse inner ear mutants and other organ

systems to unravel the mystery of otoconial development. *Brain Research*, *1091*(1), 58–74.

Inoue, M., Tanimoto, M., & Oda, Y. (2013). The role of ear stone size in hair cell acoustic sensory transduction. *Scientific Reports*, 3.

Jarvis, B. L., Johnston, M., & Sulik, K. K. (1990). Congenital malformations of the external middle, and inner ear produced by isotretinoin exposure in mouse embryos. *Otolaryngology-Head and Neck Surgery*, *102*(4), 391–401.

Kimmel, C. B., Ballard, W. W., Kimmel, S. R., Ullmann, B., & Schilling, T. F. (1995). Stages of embryonic development of the zebrafish. *Developmental Dynamics*, *203*(3), 253–310.

Liu, C., Song, G., Mao, L., Long, Y., Li, Q., & Cui, Z. (2015). Generation of an enhancer-trapping vector for insertional mutagenesis in zebrafish. *PLoS ONE*, *10*(10), e0139612.

Livak, K. J., & Schmittgen, T. D. (2001). Analysis of relative gene expression data using real-time quantitative PCR and the 2− ΔΔCT method. *Methods*, *25*(4), 402–408.

Lowery, L. A., & Sive, H. (2005). Initial formation of zebrafish brain ventricles occurs independently of circulation and requires the nagie oko and snakehead/atp1a1a. 1 gene products. *Development*, *132*(9), 2057–2067.

Lundberg, Y. W., Xu, Y., Thiessen, K. D., & Kramer, K. L. (2015). Mechanisms of otoconia and otolith development. *Developmental Dynamics*, *244*(3), 239–253.

Millimaki, B. B., Sweet, E. M., Dhason, M. S., & Riley, B. B. (2007). Zebrafish atoh1 genes: Classic proneural activity in the inner ear and regulation by Fgf and Notch. *Development*, *134*(2), 295–305.

Mu, Y., X-q, L., Zhang, B., & Du, J.- (2012). Visual input modulates audiomotor function via hypothalamic dopaminergic neurons through a cooperative mechanism. *Neuron*, *75*(4), 688–699.

Riley, B. B., Zhu, C., Janetopoulos, C., & Aufderheide, K. J. (1997). A critical period of ear development controlled by distinct populations of ciliated cells in the zebrafish. *Developmental Biology*, *191*(2), 191–201.

Roberts, R., Elsner, J., & Bagnall, M. W. (2017). Delayed otolith development does not impair vestibular circuit formation in zebrafish. *Journal of the Association for Research in Otolaryngology*, *18*(3), 415–425.

Schneeberger, E. E., & Lynch, R. D. (2004). The tight junction: A multifunctional complex. *American Journal of Physiology-Cell Physiology*, *286*(6), C1213.

Slanchev, K., Carney, T. J., Stemmler, M. P., Koschorz, B., Amsterdam, A., Schwarz, H., & Hammerschmidt, M. (2009). The epithelial cell adhesion molecule EpCAM is required for epithelial morphogenesis and integrity during zebrafish epiboly and skin development. *PLoS Genetics*, *5*(7), e1000563.

Song, G., Li, Q., Long, Y., Gu, Q., Hackett, P. B., & Cui, Z. (2012). Effective gene trapping mediated by sleeping beauty transposon. *PLoS ONE*, *7*(8), e44123.

Spring, K. R. (1998). Routes and mechanism of fluid transport by epithelia 1. *Annual Review of Physiology*, *60*(1), 105–119.

Stooke-Vaughan, G. A., Huang, P., Hammond, K. L., Schier, A. F., & Whitfield, T. T. (2012). The role of hair cells, cilia and ciliary motility in otolith formation in the zebrafish otic vesicle. *Development*, *139*(10), 1777–1787.

Thisse, C., & Thisse, B. (2008). High-resolution in situ hybridization to whole-mount zebrafish embryos. *Nature Protocols*, *3*(1), 59–69.

Trune, D. R. (2010). Ion homeostasis in the ear: Mechanisms, maladies, and management. *Current Opinion in Otolaryngology & Head and Neck Surgery*, *18*(5), 413.

Tsukita, S., Furuse, M., & Itoh, M. (2001). Multifunctional strands in tight junctions. *Nature Reviews Molecular Cell Biology*, *2*(4), 285–293.

Uren, A. G., Mikkers, H., Kool, J., van der Weyden, L., Lund, A. H., Wilson, C. H., . . . Berns, A. (2009). A high-throughput splinkerette-PCR method for the isolation and sequencing of retroviral insertion sites. *Nature Protocols*, *4*(5), 789–798.

Westerfield, M. (2000). *The zebrafish book: a guide for the laboratory use of zebrafish (Danio rerio)*. University of Oregon Press Eugene, OR.

Whitfield, T. T., Mburu, P., Hardisty-Hughes, R. E., & Brown, S. D. M. (2005). Models of congenital deafness: Mouse and zebrafish. *Drug Discovery Today: Disease Models*, *2*(2), 85–92.

Wilcox, E. R., Burton, Q. L., Naz, S., Riazuddin, S., Smith, T. N., Ploplis, B., . . . Friedman, T. B. (2001). Mutations in the gene encoding tight junction claudin-14 cause autosomal recessive deafness DFNB29. *Cell*, *104*(1), 165–172.

Wu, D., Freund, J. B., Fraser, S. E., & Vermot, J. (2011). Mechanistic basis of otolith formation during teleost inner ear development. *Developmental Cell*, *20*(2), 271–278.

Yu X, Lau D, Ng CP, & Roy S. 2011. Cilia-driven fluid flow as an epigenetic cue for otolith biomineralization on sensory hair cells of the inner ear. *Development 138*(3):487–494.

SUPPORTING INFORMATION

Additional Supporting Information may be found online in the supporting information tab for this article.

How to cite this article: Li X, Song G, Zhao Y, et al. Claudin7b is required for the formation and function of inner ear in zebrafish. *J Cell Physiol*. 2018;233:3195–3206. https://doi.org/10.1002/jcp.26162